Title

Regional stratification at the top of Earth's core due to core–mantle boundary heat flux variations

Journal

Nature Geoscience, 12(7)

ISSN

1752-0894

Authors

Mound, Jon
Davies, Chris
Rost, Sebastian
et al.

Publication Date

2019-07-01

DOI

10.1038/s41561-019-0381-z

Peer reviewed

nature geoscience

ARTICLES

https://doi.org/10.1038/s41561-019-0381-z

Regional stratification at the top of Earth's core due to core–mantle boundary heat flux variations

Jon Mound[1*], Chris Davies[1], Sebastian Rost[1] and Jon Aurnou[2]

Earth's magnetic field is generated by turbulent motion in its fluid outer core. Although the bulk of the outer core is vigorously convecting and well mixed, some seismic, geomagnetic and geodynamic evidence suggests that a global stably stratified layer exists at the top of Earth's core. Such a layer would strongly influence thermal, chemical and momentum exchange across the core–mantle boundary and thus have important implications for the dynamics and evolution of the core. Here we argue that the relevant scenario is not global stratification, but rather regional stratification arising solely from the lateral variations in heat flux at the core–mantle boundary. Using our extensive suite of numerical simulations of the dynamics of the fluid core with heterogeneous core–mantle boundary heat flux, we predict that thermal regional inversion layers extend hundreds of kilometres into the core under anomalously hot regions of the lowermost mantle. Although the majority of the outermost core remains actively convecting, sufficiently large and strong regional inversion layers produce a one-dimensional temperature profile that mimics a globally stratified layer below the core–mantle boundary—an apparent thermal stratification despite the average heat flux across the core–mantle boundary being strongly superadiabatic.

Observations of stratification at the top of the core have attracted much attention, but the results are controversial. Seismic wave speeds at the top of the core[1,2] have been matched to a compositional model[3] and interpreted as the signature of a global layer that is both thick (~300 km) and strongly stratified (Brunt–Väisälä periods of 1.63–3.43 h). Geomagnetic oscillations have been interpreted as the signature of magnetic, Archimedes and Coriolis (MAC) waves within a stratified layer ~140 km thick with a maximum Brunt–Väisälä frequency that is roughly diurnal[4,5]; although other explanations for the observed oscillations have been proposed[6]. Core flow models constructed from geomagnetic secular variation have been used to argue both for and against radial motion near the top of the core[7–10] and some seismic studies[11,12] have found that the structure of the outermost core does not require global stratification. Core stratification would also influence the long-term thermal evolution of the core[13], support a range of wave dynamics not found in a fully convecting core[14] and alter the long-term structure of the external planetary magnetic field (by suppressing radial motion near the core–mantle boundary (CMB))[15,16].

Vigorous rotationally influenced flows within the electrically conductive liquid iron outer core are essential for the continued regeneration of the Earth's magnetic field through the magneto-hydrodynamic geodynamo process. There is little doubt that the bulk of Earth's liquid core is undergoing turbulent convection and the horizontal temperature fluctuations within the adiabatically well-mixed fluid are expected to be very small (of the order of 10^{-3} K)[17]. Comparatively large radial variations in core properties may exist near the boundaries of the liquid core if some mechanism enables the generation or accumulation of fluid with a stable density stratification.

Three principle mechanisms have been invoked to explain a global non-adiabatic structure at the top of the core. The first supposes that the core has slowly cooled to a point where the heat flux, q, has fallen below the adiabatic heat flux, q_a, across the CMB[13]. This scenario produces a wide range of thickness estimates[18] that rely on the poorly known CMB heat flow and much-debated core conductivity[19]. The second mechanism invokes chemical diffusion, either along the core pressure gradient[20] or across the CMB from the mantle[21], which enriches the top of the core in light elements. The third possibility is emplacement of a light layer during core formation[22], which must then avoid disruption, by the moon-forming impact, for example, and throughout the lifetime of the Earth[23].

The top of the core will also be strongly influenced by thermal heterogeneity in the lowermost mantle, which is much stronger than in the core (of the order of 10^2 K) and evolves much more slowly, such that the mantle imposes a laterally varying pattern of heat flux across the CMB[24]. Estimates of the lateral variations in the CMB heat flux[25–27] are sufficiently large that substantial regional variations in core dynamics are expected[16,28–31]. Previous models[16,32–34] have considered the interaction between CMB heterogeneity and stratification at the top of the core and the extent to which such heterogeneity can drive flows that penetrate and possibly disrupt a global stratified layer[24,35]. Instead of viewing heterogeneous CMB heat flux as a factor acting in opposition to some mechanism of global stratification, we argue that it is the source of an apparent global stratification at the top of the core.

Using an extensive suite of non-magnetic rotating convection simulations, we are able to systematically access the strongly nonlinear, rotationally constrained, turbulent flow regime most relevant to the Earth's core. Within this regime we find that the bulk of the core remains actively convecting due to a strong net superadiabatic heat flow across the CMB and no global thermally stratified layer can form. Sufficiently warm regions in the lowermost mantle may locally reduce q below q_a, allowing regional accumulations of hot fluid at the top of the core and the formation of convectively stable regions of thermal inversion (that is, the radial temperature gradient $\partial T/\partial r$ (where T is temperature and r radius) is locally positive within these regions). The spatial extent and buoyancy anomaly of these convectively stable lenses of fluid below the CMB, which we call regional inversion layers, are primarily set by the long-wavelength,

[1]School of Earth and Environment, University of Leeds, Leeds, UK. [2]Department of Earth and Space Sciences, University of California, Los Angeles, CA, USA. *e-mail: J.E.Mound@leeds.ac.uk

high-amplitude variations in CMB heat flux imposed on the core by the mantle. Large and strong regional inversion layers can dominate the spherically averaged temperature profile resulting in an apparent thermal stratification near the top of the core. There is no doubt that the fundamental physical mechanism that underpins our scenario, namely large lateral variations in CMB heat flux, exists within the Earth[25,26,36]; the only question is how substantial its influence might be. Thick regional inversion layers are ubiquitous in our simulations and, we argue, should be expected in the Earth's core.

Modelling of regional inversion layers

We investigate regional inversion layers in the core using a suite of numerical simulations of non-magnetic rotating convection that includes two patterns (see Supplementary Fig. 1) and two amplitudes of CMB heat flux heterogeneity (see Methods and our previous work[31]). The amplitude of CMB heat flux heterogeneity in our numerical model is described by $q^* = \frac{q_{max} - q_{min}}{q_{ave}}$, where q_{max}, q_{min}, and q_{ave} are the maximum, minimum and horizontally averaged heat fluxes through the outer boundary, respectively. In this study, we consider strong lateral variations in CMB heat flux with $q^* = \{2.3, 5.0\}$. One pattern of CMB heat flux heterogeneity is derived from seismic tomography[36]. Laterally and radially extensive regions of low seismic velocity in the lowermost mantle, termed large low velocity provinces (LLVPs), have been observed and are hypothesized to arise from either thermal or thermochemical mechanisms[37]. In either case, these regions are expected to be anomalously warm and impose a reduced CMB heat flux on the core beneath Africa and the Pacific. The second is a hemispheric pattern that could represent the configuration of mantle flow during times of supercontinent formation. For our chosen hemispheric pattern, q_{min} is located under Null Island (0° N, 0° E).

Numerical models of core convection can be characterized by three control parameters: the Prandtl number (Pr), which is the ratio of the fluid's viscous and thermal diffusivities; and the (modified) Rayleigh number (Ra)and Ekman number (E), which primarily reflect balances between rotational, viscous and buoyancy forces. Theoretical considerations based on the force balance between inertia, viscosity and rotation suggests that the dynamic regime should be characterized using the Reynolds number, $\mathrm{Re} = UL/\nu$, and Rossby number, $\mathrm{Ro} = U/2\Omega L = \mathrm{Re}E$, where U and L are the characteristic velocity and length scale of the flow, respectively, ν is the momentum diffusivity and Ω is the planetary rotation rate. Our simulations consider higher modified Ra and lower E than previous models that incorporate CMB heat flux heterogeneity[16,29,30]. In particular, values of $E < 10^{-4}$ allow us to access the regime of rapidly rotating convection[31,38]. We also restrict our attention to simulations for which Ra is at least ten times greater than the critical Ra for the onset of convection Ra_c to ensure that we have left the weakly nonlinear regime near the onset of convection. Crucially, our choice of control parameters results in the fluid flow in our simulations being both turbulent (large Re) and strongly influenced by rotation (small Ro) as in Earth's core (Table 1).

We find that convectively stable regions of thermal inversion ($\partial T/\partial r > 0$) can be maintained over large lateral and radial extents in all of our simulations, although the bulk of the core remains strongly convecting and hence well mixed on short length scales (Figs. 1 and 2). The sizes of the regional inversion layers are associated with the long wavelengths of the imposed boundary heterogeneity rather than the small wavelengths of the convecting core (Fig. 1, Supplementary Fig. 2, Supplementary Videos 1 and 2). Indeed, the small scale fluctuations associated with strongly supercritical convection inhibit their ability to disrupt the large regions of thermal inversion[39]. Previous studies at low Ra did not find the stratification signal[29], perhaps because the potentially stable regions were disrupted by the large-scale convective patterns that arise close to onset.

Table 1 | Non-dimensional numbers

Quantity	Definition	Molecular diffusivities	Turbulent diffusivities	Simulations
Rayleigh	$\mathrm{Ra} = \frac{\alpha g_0 \beta}{2\Omega\kappa}$	4×10^{13}	2×10^{10}	225–18,000
Ekman	$E = \frac{\nu}{2\Omega L^2}$	7×10^{-16}	4×10^{-11}	10^{-6}–10^{-4}
Prandtl	$\mathrm{Pr} = \frac{\nu}{\kappa}$	0.04	1	1
Reynolds	$\mathrm{Re} = UL/\nu$	2×10^{9}	4×10^{4}	10^{1}–10^{3}
Rossby	$\mathrm{Ro} = U/2\Omega L = \mathrm{Re}E$	1.5×10^{-6}	1.5×10^{-6}	10^{-4}–10^{-1}

Regional inversion layers form underneath areas where the local CMB heat flux is sufficiently low to suppress convection near the top of the core. For our patterns of heterogeneity (Supplementary Fig. 1), the CMB heat flux minima occur at or near the Equator and thus the geographic profiles investigated in Figs. 2 and 3 focus on these regions. An inversion layer can exist a few hundred kilometres below the CMB even where the CMB heat flux remains superadiabatic, as azimuthal flow sweeps hot material horizontally; see, for example, the volume of fluid with $\partial T/\partial r > 0$ that extends west from the Pacific in Fig. 1. Enhanced CMB heat flux, relative to that underneath the LLVP, cools this westward extension of the Pacific inversion layer from above until the fluid becomes locally unstable with respect to thermal convection and mixes back into the bulk (see Supplementary Video 1).

The strength of the thermal inversion is characterized by the maximum Brunt–Väisälä frequency (N), which we normalize relative to 2Ω. Scaling analysis (see Methods) shows that the strength of the inversion should vary as

$$\left.\frac{N}{2\Omega}\right|_{max} \approx \left(\frac{1}{r_o^*}\right)\sqrt{\frac{\mathrm{Ra}E}{\mathrm{Pr}}\left(\frac{q^*-2}{2}\right)} \quad (1)$$

where r_o^* is the dimensionless CMB radius. Extrapolation to the Earth must therefore account for both the increase in Ra and the decrease in E relative to numerical simulations (Table 1). Stronger boundary heterogeneity (larger q^*) implies more anomalous $\partial T/\partial r$ at the CMB and we expect N^2 to increase in proportion to q^*.

The value of q^* can be estimated from first-principles calculations of thermal conductivity coupled to seismic tomographic models[26], which suggest that heat flux across the CMB ranges from roughly 0–140 mW m^{-2}. Much of the net radial heat flow within the core occurs due to conduction along the adiabatic temperature gradient[19]; this contribution needs to be removed when considering the relation between our Boussinesq model and the Earth. The superadiabatic heat flow across the CMB has been estimated as 0.6 TW based on a theoretical scaling between inertial and buoyancy forces in rotating convection[17]. These values suggest that q^* for the Earth may be as large as ~35, in which case $N/2\Omega \approx 2$ is predicted for the Earth for reasonable estimates of other physical parameters (Supplementary Table 1).

No theoretical scaling exists for the thickness of the regional inversion layers; they are not simple boundary layers, which would thin both as Ra is increased and as E is decreased towards Earth-like values. Instead we find a competition between thinner layers as E is reduced, but generally thicker layers as Ra is increased for a given choice of q^* and CMB heat-flux pattern (Fig. 2 and Supplementary Figs. 2 and 3).

Regional inversion layers that are both thick (several hundred kilometres) and strong ($N/2\Omega \approx 10^{-2}$–$10^{0}$) are ubiquitous in our models. The derived expression for Brunt–Väisälä frequency (equation 1) suggests that regional thermal stratification should be expected at

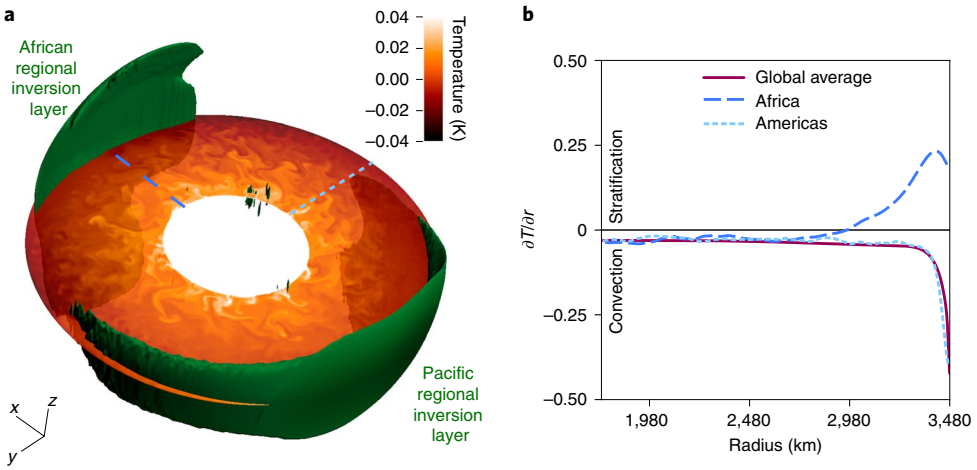

Fig. 1 | Thermal structure in a simulation with a tomographic pattern of CMB heat flux. $q^*=5.0$, $E=10^{-6}$ and $\mathrm{Ra}=1.8\times10^4$. **a**, Green isovolumes denote convectively stable regions of positive $\partial T/\partial r$ in the time average; the equatorial slice shows the temperature anomaly field at one point in time. **b**, Time-averaged profiles of $\partial T/\partial r$ in the top half of the outer core. Regional profiles on the equator ($\theta=\pi/2$) are shown for longitudes associated with Africa ($\phi=0$) and the Americas ($\phi=3\pi/2$). The horizontally averaged profile is shown by the solid purple line. Temperature has been non-dimensionalized as described in the Methods.

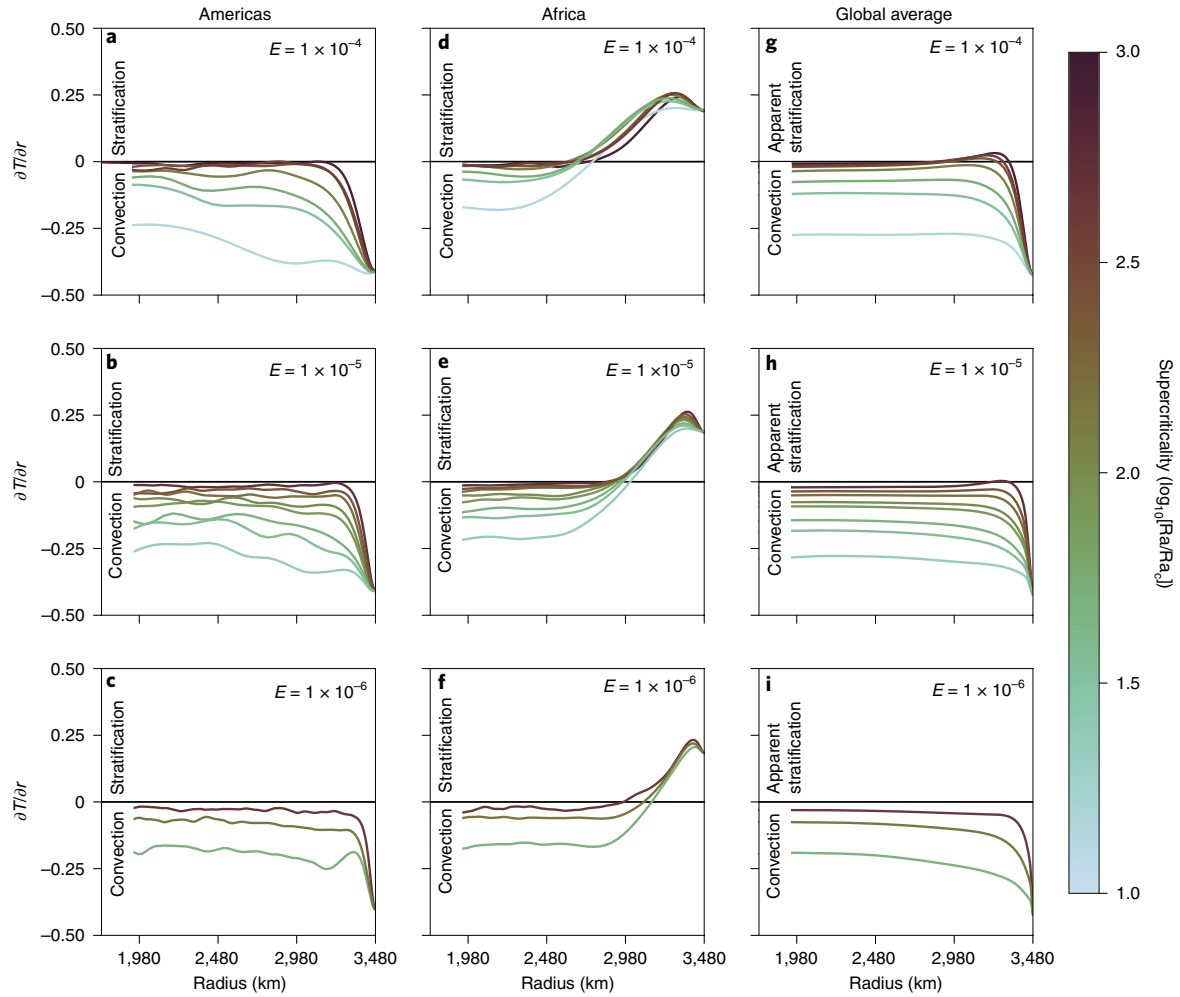

Fig. 2 | Profiles of the time-averaged temperature gradient in the top half of the core. a–i, As in Fig. 1, we consider equatorial profiles under the Americas (**a**–**c**) and Africa (**d**–**f**), as well as the global average (**g**–**i**). Simulations have a tomographic CMB heat flux pattern, with $q^*=5.0$ and $E=10^{-4}$ (**a**,**d**,**g**), 10^{-5} (**b**,**e**,**h**), or 10^{-6} (**c**,**f**,**i**). The colours of the curves indicate the supercriticality of the modified Ra from 10 times critical (light shades) to 1,000 times critical (dark shades, see colour scale). Temperature has been non-dimensionalized as described in the Methods.

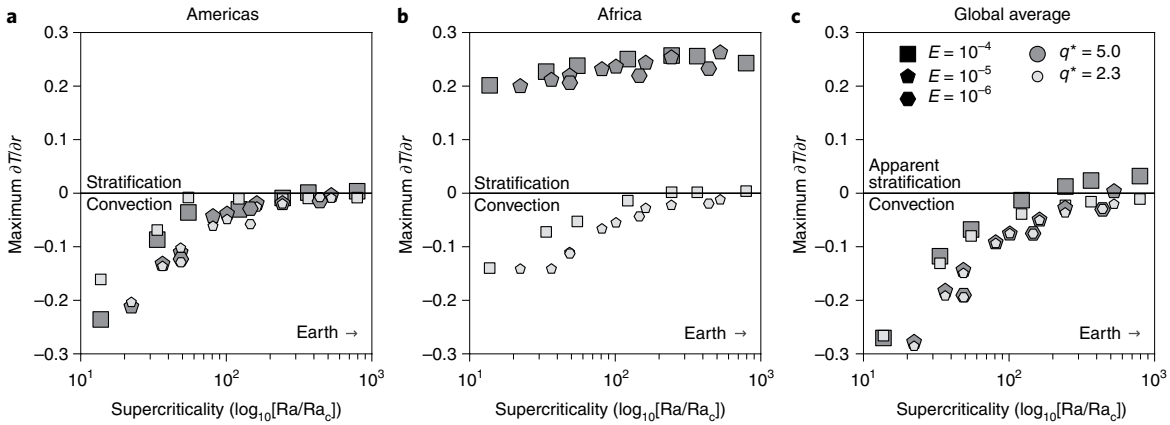

Fig. 3 | The thermal signature of stratification. The maxima of the profiles of the time-averaged temperature gradient (Fig. 2) are plotted as a function of supercriticality. As supercriticality increases, the temperature gradient maxima in our simulations become more positive, corresponding to the formation and strengthening of regional inversion layers and apparent global stratification. **a**–**c**, Equatorial profiles under the Americas (**a**) and Africa (**b**) and the global average (**c**). Simulations have a tomographic pattern of CMB heat flux; the symbol size and shade indicate q^*.

low E, provided Ra is sufficently large and q^* is greater than two. If the regional inversion layers are sufficiently large and strong, the horizontally averaged temperature gradient near the top of the core can become positive (Figs. 2 and 3), an apparent global stratification despite the average heat flux across the CMB being strongly superadiabatic. This apparent global stratification signal becomes stronger as Ra is increased and the bulk of the core becomes more isothermal, thereby causing the horizontally averaged temperature gradient near the top of the core to be increasingly dominated by the large gradients that exist in the regional inversion layers.

Implications for Earth

Previous dynamical modelling[16,24,32–35] has focused on interactions between heterogeneous boundary conditions and global stratified layers at the top of the core, motivated by assumptions that uniform compositional enrichment[20–22] or net subadiabatic CMB heat flux[13,18] are driving stratification. In contrast, our simulations do not impose a net stratification as they are all strongly supercritical and have a completely well-mixed fluid core in the absence of CMB heterogeneity. However, thermal variations in Earth's lowermost mantle are sufficiently strong that large areas of the CMB are expected to have a subadiabatic heat flux[25,26,36]. Such areas locally inhibit convection in the outermost core, although the bulk of the core remains vigorously convecting. Apparent global stratification arises as a consequence of CMB heterogeneity when the regional inversion layers control the sign of the global average radial temperature gradient, which is particularly likely at the high-Ra conditions relevant to the Earth. The strength and extent of these regions is set by the boundary heterogeneity, which is faithfully represented in our simulations; we argue that broad and thick regional inversion layers should therefore be expected in the Earth.

For the present day Earth, the CMB heat flux is particularly low under the African and Pacific LLVPs and thus regional inversion layers are expected to be most prominent in these equatorial regions. If mantle convection in the geological past had an approximately hemispheric pattern[40], then the regional inversion layers at those times would be expected to have a hemispheric pattern (see Supplementary Figs. 2 and 3). The distribution of regional inversion layers in the past might be reflected in other large-scale core processes that have been linked to mantle control, such as the structure and reversal rate of the magnetic field[27,41,42] and the (possibly asymmetric) growth of the inner core[27,43,44].

Unlike our Boussinesq numerical model, the anomalous regions in Earth's core need not have a strictly positive thermal gradient—they need only have a subadiabatic gradient that is dynamically distinct from the bulk of the core. The temperature difference between the top of actively convecting regions and the regional inversion layers depends on the layer thickness, q^* and the net superadiabatic heat flow across the CMB. By assuming purely thermal convection, a simple theoretical analysis suggests that the boundary-forced temperature variations can be orders of magnitude larger than those associated with the free convection (see Methods, Supplementary Fig. 5); however, temperature is believed to have only a moderate impact on seismic velocity in the core[45]. Chemical variations are expected to have a larger impact, but the resultant seismic velocity relies on uncertain properties such as the core's bulk composition, the nature of any chemical variation and the impact of different chemical species on the bulk modulus and density[3,46,47]. Our simulations are designed to elucidate the fluid dynamics of regional inversion layer formation due to CMB heat flux heterogeneity and provide a basis for future models that may incorporate processes such as barodiffusion, chemical exchange across the CMB and primordial stratification, which have been hypothesized to influence the composition of the outermost core.

Although radial motion would be inhibited within a strongly stratified global layer, the regional inversion layers in our simulations are dynamically connected to the rest of the core; thus radial velocity is not completely suppressed within them (Fig. 4). The lateral variations in CMB heat flux drive thermal winds that sweep hot material out from under the locally stable regions of low CMB heat flux, enabling it to cool and mix back into the vigorously convecting bulk. This results in broad, weak upwellings through the regional inversion layers in our simulations. In the Earth, strong thermal winds would also be expected and such boundary-driven flows have been used in previous dynamo studies[48–50] to explain long-term non-axisymmetric features of the geomagnetic field. A simple extrapolation of the thermal wind balance suggests velocities of the order of $1\,\mathrm{mm\,s^{-1}}$ at a depth of a few hundred metres, comparable to the velocities inferred for the top of the core from geomagnetic observations[10]. At greater depths, the thermal winds would be proportionally stronger, reaching the order of $1\,\mathrm{m\,s^{-1}}$ a few hundred kilometres below the CMB—considerably faster than observational constraints. However, deep jets with such large peak velocities may not develop in Earth's core, where the thermal wind balance is modified by magnetic field effects[24].

Regional inversion layers may influence observable geomagnetic variation as both the wave dynamics and fluid flow (Fig. 4) in these regions would have a different character to that in the bulk of the

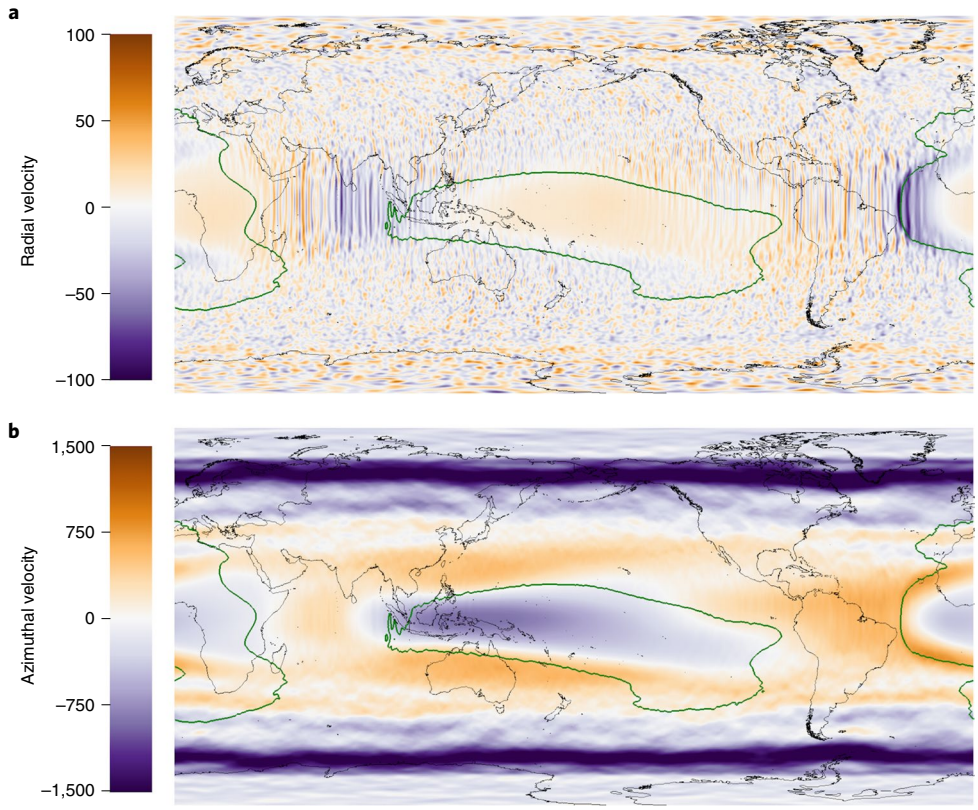

Fig. 4 | Flow ~100 km below the CMB. a,**b**, Time-averaged radial velocity (**a**), azimuthal velocity (**b**) and contours of $\partial T/\partial r = 0$ (green) for the simulation in Fig. 1. The averaging was done over 37 advection times. The flow velocity is non-dimensionalized as described in the Methods.

core. Hemispheric patterns in geomagnetic secular variation[51] may suggest that only one dominant regional inversion layer is present. In our model the LLVPs are associated with low CMB heat flux and thus regional inversion layers; however, the latitudinal and longitudinal extents of the two LLVPs are quite different, which could result in differing influences on core thermal structure and hence geomagnetic variation. A hemispheric difference could also arise due to differences in temperature between the Pacific and African LLVPs, which might reflect differing balances between thermal and chemical contributions to the origin of these LLVPs. We find that the CMB heat flux reduction predicted by our chosen tomographic model is greater under the Pacific LLVP and this regional inversion layer tends to form more readily and be more extensive than the African LLVP. A hemispheric difference at the top of the core might therefore indicate that the average heat flux across the CMB is sufficiently high to prevent regional inversion under Africa but not the Pacific. Uneven growth of the inner core[52,53] might also produce large length scale differences in core dynamics that could influence hemispheric structures and dynamics at the top of the core[49,50,54].

Without sufficient geographic coverage or understanding of how the path-integrated delay of SmKS phases are influenced by regional inversion layers (for example, from 3D wave-propagation models), studies of average structure might well mistake extensive regional inversion layers for global stratification. The geometry and strength of regional inversion layers in the core depend on the pattern and amplitude of the imposed heat flux heterogeneity, which is set by the distributions of both temperature and thermal conductivity in the lowermost mantle. The extent of the regional inversion layers varies considerably within our simulations, but the location of the thickest anomalous structure is generally centred under the mantle LLVPs. By contrasting SmKS paths that are expected to completely avoid regional inversion layers with those that should sample the middle of them, it may be possible to test whether the average seismic structure at the top of the core is truly the result of global stratification or if it is instead the signature of large boundary-forced regional inversion layers.

Online content

Any methods, additional references, Nature Research reporting summaries, source data, statements of code and data availability and associated accession codes are available at https://doi.org/10.1038/s41561-019-0381-z.

Received: 10 September 2018; Accepted: 2 May 2019;
Published online: 17 June 2019

References

1. Lay, T. & Young, C. J. The stably-stratified outermost core revisited. *Geophys. Res. Lett.* **17**, 2001–2004 (1990).
2. Kaneshima, S. Array analyses of SmKS waves and the stratification of Earth's outermost core. *Phys. Earth Planet. Inter.* **276**, 234–246 (2018).
3. Helffrich, G. & Kaneshima, S. Outer-core compositional stratification from observed core wave speed profiles. *Nature* **468**, 807–810 (2010).
4. Buffett, B. Geomagnetic fluctuations reveal stable stratification at the top of the Earth's core. *Nature* **507**, 484–487 (2014).
5. Buffett, B., Knezek, N. & Holme, R. Evidence for mac waves at the top of Earth's core and implications for variations in length of day. *Geophys. J. Int.* **204**, 1789–1800 (2016).
6. Buffett, B. A., Mound, J. & Jackson, A. Inversion of torsional oscillations for the structure and dynamics of Earth's core. *Geophys. J. Int.* **177**, 878–890 (2009).
7. Whaler, K. A. Does the whole of the Earth's core convect? *Nature* **287**, 528–530 (1980).
8. Gubbins, D. Geomagnetic constraints on stratification at the top of Earth's core. *Earth Planets Space* **59**, 661–664 (2007).
9. Amit, H. Can downwelling at the top of the Earth's core be detected in the geomagnetic secular variation? *Phys. Earth Planet. Inter.* **229**, 110–121 (2014).
10. Lesur, V., Whaler, K. & Wardinski, I. Are geomagnetic data consistent with stably stratified flow at the core-mantle boundary? *Geophys. J. Int.* **201**, 929–946 (2015).

11. Alexandrakis, C. & Eaton, D. W. Precise seismic-wave velocity atop Earth's core: no evidence for outer-core stratification. *Phys. Earth Planet. Inter.* **180**, 59–65 (2010).
12. Irving, J. C. E., Cottaar, S. & Lekić, V. Seismically determined elastic parameters for Earth's outer core. *Sci. Adv.* **4**, 1–9 (2018).
13. Lister, J. R. & Buffett, B. A. Stratification of the outer core at the core-mantle boundary. *Phys. Earth Planet. Inter.* **105**, 5–19 (1998).
14. Braginsky, S. I. Dynamics of the stably stratified ocean at the top of the core. *Phys. Earth Planet. Inter.* **111**, 21–34 (1999).
15. Christensen, U. R. & Wicht, J. Models of magnetic field generation in partly stable planetary cores: applications to Mercury and Saturn. *Icarus* **196**, 16–34 (2008).
16. Olson, P., Landeau, M. & Reynolds, E. Dynamo tests for stratification below the core-mantle boundary. *Phys. Earth Planet. Inter.* **271**, 1–18 (2017).
17. Jones, C. A. Planetary magnetic fields and fluid dynamos. *Annu. Rev. Fluid Mech.* **43**, 583–614 (2011).
18. Gubbins, D., Alfè, D., Davies, C. & Pozzo, M. On core convection and the geodynamo: effects of high electrical and thermal conductivity. *Phys. Earth Planet. Inter.* **247**, 56–64 (2015).
19. Davies, C., Pozzo, M., Gubbins, D. & Alfè, D. Constraints from material properties on the dynamics and evolution of Earth's core. *Nat. Geosci.* **8**, 678–685 (2015).
20. Gubbins, D. & Davies, C. J. The stratified layer at the core-mantle boundary caused by barodiffusion of oxygen, sulphur and silicon. *Phys. Earth Planet. Inter.* **215**, 21–28 (2013).
21. Buffett, B. A. & Seagle, C. T. Stratification of the top of the core due to chemical interactions with the mantle. *J. Geophys. Res.* **115**, B04407 (2010).
22. Landeau, M., Olson, P., Deguen, R. & Hirsh, B. H. Core merging and stratification following giant impact. *Nat. Geosci.* **9**, 786–789 (2016).
23. Jacobson, S. A., Rubie, D. C., Hernlund, J., Morbidelli, A. & Nakajima, M. Formation, stratification, and mixing of the cores of Earth and Venus. *Earth Planet. Sci. Lett.* **474**, 375–386 (2017).
24. Lister, J. R. Thermal winds forced by inhomogeneous boundary conditions in rotating, stratified, hydromagnetic fluid. *J. Fluid Mech.* **505**, 163–178 (2004).
25. Nakagawa, T. & Tackley, P. J. Lateral variations in CMB heat flux and deep mantle seismic velocity caused by a thermal–chemical-phase boundary layer in 3D spherical convection. *Earth Planet. Sci. Lett.* **271**, 348–358 (2008).
26. Stackhouse, S., Stixrude, L. & Karki, B. B. First-principles calculations of the lattice thermal conductivity of the lower mantle. *Earth Planet. Sci. Lett.* **427**, 11–17 (2015).
27. Olson, P., Deguen, R., Rudolph, M. L. & Zhong, S. Core evolution driven by mantle global circulation. *Phys. Earth Planet. Inter.* **243**, 44–55 (2015).
28. Gibbons, S. J., Gubbins, D. & Zhang, K. Convection in rotating spherical fluid shells with inhomogeneous heat flux at the outer boundary. *Geophys. Astrophys. Fluid Dynam.* **101**, 347–370 (2007).
29. Davies, C. J., Gubbins, D. & Jimack, P. K. Convection in a rapidly rotating spherical shell with an imposed laterally varying thermal boundary condition. *J. Fluid Mech.* **641**, 335–358 (2009).
30. Dietrich, W., Hori, K. & Wicht, J. Core flows and heat transfer induced by inhomogeneous cooling with sub- and supercritical convection. *Phys. Earth Planet. Inter.* **251**, 36–51 (2016).
31. Mound, J. E. & Davies, C. J. Heat transfer in rapidly rotating convection with heterogeneous thermal boundary conditions. *J. Fluid Mech.* **828**, 601–629 (2017).
32. Sreenivasan, B. & Gubbins, D. Dynamos with weakly convecting outer layers: implications for core-mantle boundary interaction. *Geophys. Astrophys. Fluid Dynam.* **102**, 395–407 (2008).
33. Sahoo, S., Sreenivasan, B. & Amit, H. Dynamos driven by weak thermal convection and heterogeneous outer boundary heat flux. *Phys. Earth Planet. Inter.* **250**, 35–45 (2016).
34. Olson, P., Landeau, M. & Reynolds, E. Outer core stratification from the high latitude structure of the geomagnetic field. *Front. Earth Sci.* **6**, 1–13 (2018).
35. Christensen, U. R. Geodynamo models with a stable layer and heterogeneous heat flow at the top of the core. *Geophys. J. Int.* **215**, 1338–1351 (2018).
36. Masters, G., Johnson, S., Laske, G. & Bolton, H. A shear-velocity model of the mantle. *Phil. Trans. R. Soc. A* **354**, 1385–1411 (1996).
37. Hernlund, J. W. & McNamara, A. K. in *Mantle Dynamics* (ed. Bercovici, D.) 461–519 (Elsevier, 2015).
38. Gastine, T., Wicht, J. & Aubert, J. Scaling regimes in spherical shell rotating convection. *J. Fluid Mech.* **808**, 690–732 (2016).
39. Calkins, M. A. et al. The asymptotic equivalence of fixed heat flux and fixed temperature thermal boundary conditions for rapidly rotating convection. *J. Fluid Mech.* **784**, R2 (2015).
40. Zhang, N. & Zhong, S. Heat fluxes at the Earth's surface and core–mantle boundary since Pangea formation and their implications for the geomagnetic superchrons. *Earth Planet. Sci. Lett.* **306**, 205–216 (2011).
41. Glatzmaier, G. A., Coe, R. S., Hongre, L. & Roberts, P. H. The role of the Earth's mantle in controlling the frequency of geomagnetic reversals. *Nature* **401**, 885–890 (1999).
42. Olson, P., Deguen, R., Hinnov, L. A. & Zhong, S. Controls on geomagnetic reversals and core evolution by mantle convection in the Phanerozoic. *Phys. Earth Planet. Inter.* **214**, 87–103 (2013).
43. Aubert, J., Amit, H., Hulot, G. & Olson, P. Thermochemical flows couple the Earth's inner core growth to mantle heterogeneity. *Nature* **454**, 758–761 (2008).
44. Gubbins, D., Sreenivasan, B., Mound, J. & Rost, S. Melting of the Earth's inner core. *Nature* **473**, 361–363 (2011).
45. Ichikawa, H., Tsuchiya, T. & Tange, Y. The P-V-T equation of state and thermodynamic properties of liquid iron. *J. Geophys. Res.* **119**, 240–252 (2014).
46. Komabayashi, T. Thermodynamics of melting relations in the system Fe-FeO at high pressure: implications for oxygen in the Earth's core. *J. Geophys. Res. Solid Earth* **119**, 4164–4177 (2014).
47. Brodholt, J. & Badro, J. Composition of the low seismic velocity *E*' layer at the top of Earth's core. *Geophys. Res. Lett.* **44**, 8303–8310 (2017).
48. Olson, P. & Christensen, U. R. The time-averaged magnetic field in numerical dynamos with non-uniform boundary heat flow. *Geophys. J. Int.* **151**, 809–823 (2002).
49. Aubert, J., Finlay, C. C. & Fournier, A. Bottom-up control of geomagnetic secular variation by the Earth's inner core. *Nature* **502**, 219–223 (2013).
50. Mound, J., Davies, C. & Silva, L. Inner core translation and the hemispheric balance of the geomagnetic field. *Earth Planet. Sci. Lett.* **424**, 148–157 (2015).
51. Finlay, C. C., Olsen, N., Kotsiaros, S., Gillet, N. & Tøffner-Clausen, L. Recent geomagnetic secular variation from Swarm and ground observatories as estimated in the CHAOS-6 geomagnetic field model. *Earth, Planets Space* **68**, 112 (2016).
52. Alboussière, T., Deguen, R. & Melzani, M. Melting-induced stratification above the Earth's inner core due to convective translation. *Nature* **466**, 744–747 (2010).
53. Monnereau, M., Calvet, M., Margerin, L. & Souriau, A. Lopsided growth of Earth's inner core. *Science* **328**, 1014–1017 (2010).
54. Davies, C. J., Silva, L. & Mound, J. On the influence of a translating inner core in models of outer core convection. *Phys. Earth Planet. Inter.* **214**, 104–114 (2013).

Acknowledgements

C.D. is supported by a Natural Environment Research Council Independent Research Fellowship (NE/L011328/1). J.A. is supported by the NSF Geophysics programme via award no. EAR-1853196. This work used the ARCHER UK National Supercomputing Service (http://www.archer.ac.uk) and ARC2, part of the High Performance Computing facilities at the University of Leeds, UK.

Author contributions

All authors discussed and developed the central ideas and contributed to the writing of the manuscript. J.M. and C.D. carried out the numerical modelling and analysis.

Competing interests

The authors declare no competing interests.

Additional information

Supplementary information is available for this paper at https://doi.org/10.1038/s41561-019-0381-z.

Reprints and permissions information is available at www.nature.com/reprints.

Correspondence and requests for materials should be addressed to J.M.

Publisher's note: Springer Nature remains neutral with regard to jurisdictional claims in published maps and institutional affiliations.

Methods

Governing equations and parameter regime. We employ a numerical model of non-magnetic rotating convection of a homogeneous Boussinesq fluid confined within a rotating spherical shell[55], with fixed-flux thermal boundary conditions and no slip velocity boundary conditions. In non-dimensional form the conservation equations for momentum, energy, and mass are

$$\frac{E}{\mathrm{Pr}}\left(\frac{\partial \mathbf{u}}{\partial t}+(\mathbf{u}\cdot\nabla)\mathbf{u}\right)+\hat{\mathbf{z}}\times\mathbf{u}=-\nabla P+\mathrm{Ra}T'\mathbf{r}+E\nabla^2\mathbf{u} \quad (2)$$

$$\frac{\partial T}{\partial t}+(\mathbf{u}\cdot\nabla)T=\nabla^2 T \quad (3)$$

$$\nabla\cdot\mathbf{u}=0 \quad (4)$$

where $\mathbf{u}$ and T are the velocity and temperature fields, respectively, and T' are the temperature fluctuations relative to the steady-state temperature profile in the absence of flow. The pressure term, P, includes the centrifugal potential. The fluid is characterized by its constant thermal expansion, α, thermal diffusivity, κ, kinematic viscosity, ν, and reference density, ρ_0. The fluid shell is defined by its inner and outer boundaries, r_i and r_o, respectively, and rotates with a constant angular velocity $\mathbf{\Omega}=\Omega\hat{\mathbf{z}}$. Gravity varies with radius according to $\mathbf{g}=-(g_o/r_o)\mathbf{r}$, where g_o is the magnitude of the gravitational acceleration on the outer boundary. We have non-dimensionalized using the shell thickness $L=r_o-r_i$ for the length scale, the thermal diffusion time $\tau=L^2/\kappa$ for the time scale, and β/L for the temperature scale, where $\beta=Q/4\pi k$, Q is the total heat flow through the outer boundary, $k=\kappa\rho_0 C_p$ is the thermal conductivity and C_p the heat capacity of the fluid. The resulting control parameters are Pr, E and modified Ra. The amplitude of the heterogeneity in our heat flux boundary condition is measured by $q^*=(q_{max}-q_{min})/q_{ave}$, where $q_{ave}=\frac{1}{4\pi r_o^2}\iint q\,\mathrm{d}S=Q/4\pi r_o^2$ is the horizontally averaged CMB heat flux.

Our previous study[31] includes a suite of 106 simulations with values of $q^*=\{0.0, 2.3, 5.0\}$, $\mathrm{Pr}=1$, $E=\{10^{-4},10^{-5},10^{-6}\}$ and modified Ra up to ~800 times Ra_c. The value of Ra_c increases as E is reduced and has values of $\mathrm{Ra}_c=\{16.4, 24.7, 41.0\}$ for the three values of E that we use. Here we include six more simulations with the hemispheric boundary forcing and $E=10^{-6}$. We do not include results from our simulations that have homogeneous CMB boundary heat flux ($q^*=0.0$) as these do not form regional inversion layers. Simulations with $\mathrm{Ra}<10\mathrm{Ra}_c$ do form thick regional inversion layers (see Supplementary Figs. 3 and 4); however, they have not clearly left the weakly nonlinear regime[31,38] and seem to scale differently than simulations at higher Ra. For simplicity, we focus in the main text on cases with modified $\mathrm{Ra}>10\mathrm{Ra}_c$, leaving a total of 68 simulations.

The pattern and amplitude of Earth's CMB heat flux variations are difficult to estimate because they must be inferred from seismic tomography while accounting for possible compositional effects and phase changes in the lower mantle. Nevertheless, several studies[25–27] have found a minimum heat flux of $q_{min}\approx 0\,\mathrm{mW\,m^{-2}}$, while q_{max} could rise above $200\,\mathrm{mW\,m^{-2}}$. The adiabatic gradient at the CMB is $\partial T_a/\partial r=g\gamma T/\phi\approx -0.875\pm0.125\,\mathrm{K\,km^{-1}}$ with the seismic parameter ϕ and gravity g taken from PREM[56] and the Grüneisen parameter $\gamma=1.3$–1.5 spanning the available estimates[45]. Using low[57] and high[19] thermal conductivity values, the plausible range of adiabatic heat flux is $q_a=-k\partial T_a/\partial r=15$–$100\,\mathrm{mW\,m^{-2}}$ and therefore hot regions of the lower mantle will result in a subadiabatic heat flux across the CMB. The relative strength of CMB anomalies is often measured by the parameter $q^*=(q_{max}-q_{min})/(q-q_a)$, which can take either sign given estimates[58] of $q=30$–$110\,\mathrm{mW\,m^{-2}}$. Here we are interested in the case $q^*>0$, as q^* of at least order 1 is expected within the Earth[26] and it could be much larger (indeed q^* is unbounded as q approaches q_a). If q^* is large, as is expected for the Earth, thermal boundary forcing should exert a substantial influence on core convection[59].

Brunt–Väisälä frequency. The frequency of oscillation of a radially displaced fluid parcel within a layer that has a stable density stratification ($\partial\rho/\partial r<0$) is known as the buoyancy or Brunt–Väisälä frequency and is defined by

$$N=\sqrt{-\frac{g}{\rho_0}\frac{\partial\rho}{\partial r}}=\sqrt{g\alpha\frac{\partial T}{\partial r}} \quad (5)$$

if the density anomalies arise due to purely thermal effects. Non-dimensionalizing frequency by 2Ω, in combination with our temperature and distance scalings, gives

$$\frac{N}{2\Omega}=\sqrt{\frac{g\alpha\beta}{4\Omega^2L^2}\frac{\partial T^*}{\partial r^*}}\approx\sqrt{\frac{\mathrm{Ra}E}{\mathrm{Pr}}\frac{\partial T^*}{\partial r^*}} \quad (6)$$

where T^* and r^* are non-dimensional temperature and radius, respectively.

The steepest temperature gradient within a regional inversion layer corresponds to the maximum buoyancy frequency and we expect that the steepest gradient near the top of the core is close to that set by q_{min} of the imposed CMB heat flux. However, along some radial profiles (for example, Africa, Fig. 2) the maximum of $\partial T/\partial r$ occurs some depth below the CMB. A simple pattern of heat flux heterogeneity would have $q_{ave}=(q_{max}+q_{min})/2$ and from the definition of our boundary conditions $q_{ave}=k\beta/r_o^2$; therefore we expect

$$\left.\frac{N}{2\Omega}\right|_{max}\approx\left(\frac{1}{r_o^*}\right)\sqrt{\frac{\mathrm{Ra}E}{\mathrm{Pr}}\left(\frac{q^*-2}{2}\right)} \quad (7)$$

Boundary-forced lateral temperature variations. In a fully convecting core an adiabatic temperature gradient ($\partial T_a/\partial r$) will extend from the inner core boundary to the CMB, except within thin boundary layers: a shallower conductive profile ($\mathrm{d}T_c/\mathrm{d}r$) will exist within a regional inversion layer. The temperature difference at the CMB between a fully convecting region and the top of a regional inversion layer of thickness h will be approximately

$$\delta T\approx h(\partial T_a/\partial r-\mathrm{d}T_c/\mathrm{d}r) \quad (8)$$

Setting the conductive temperature gradient throughout the inversion layer equal to the minimum CMB heat flux gives

$$\delta T\approx\frac{h}{k}(q_a-q_{min}) \quad (9)$$

To estimate δT for the Earth, we use $q^*=(q_{max}-q_{min})/(q-q_a)$ and $q-q_a=Q_{conv}/4\pi r_o^2$ to rewrite equation (9) as

$$\delta T\approx\frac{hQ_{conv}}{4\pi r_o^2 k}\left(\frac{q^*-2}{2}\right) \quad (10)$$

The thickness of the regional inversion layers arises dynamically in our models and depends on both q^* and Q_{conv}. Here we assume a superadiabatic heat flow of $Q_{conv}=0.6\,\mathrm{TW}$ and $k=100\,\mathrm{W\,m^{-1}\,K^{-1}}$ and simply vary q^* and h to estimate the temperature difference at the CMB between fully convecting and subadiabatic regions. The likely values of δT are generally on the order of tens of kelvin (Supplementary Fig. 4). The largest values correspond to particularly thick layers that will have a large Brunt–Väisälä frequency. To explain a layer with $N\approx\Omega$ by purely thermal effects requires $\partial T/\partial r\approx 35\,\mathrm{mK\,km^{-1}}$, with the temperature gradient scaling as N^2. Any compositional contribution would reduce the required temperature gradient for a given buoyancy frequency.

Figures were produced using VisIt v.2.10.2 (ref. [60]), Matplotlib v.3.0.0 (ref. [61]) and seaborn v.0.8.0[62].

Data availability

The data that support the findings of this study are available from the corresponding author on request.

Code availability

The code used to model the core dynamics is described in Willis et al.[55] and is available on request from the corresponding author.

References

55. Willis, A. P., Sreenivasan, B. & Gubbins, D. Thermal core–mantle interaction: exploring regimes for 'locked' dynamo action. *Phys. Earth Planet. Inter.* **165**, 83–92 (2007).
56. Dziewonski, A. M. & Anderson, D. L. Preliminary reference Earth model. *Phys. Earth Planet. Inter.* **25**, 297–356 (1981).
57. Konôpková, Z., McWilliams, R. S., Gómez-Pérez, N. & Goncharov, A. F. Direct measurement of thermal conductivity in solid iron at planetary core conditions. *Nature* **534**, 99–101 (2016).
58. Nimmo, F. in *Core Dynamics* (ed. Olson, P.) 27–55 (Elsevier, 2015).
59. Sumita, I. & Olson, P. Rotating thermal convection experiments in a hemispherical shell with heterogeneous boundary heat flux: implications for the Earth's core. *J. Geophys. Res.* **107**, 2169 (2002).
60. Childs, H. et al. in *High Performance Visualization* (eds Bethel, E. W. et al.) 357–372 (Chapman and Hall, 2012).
61. Hunter, J. D. Matplotlib: A 2D graphics environment. *Comput. Sci. Eng.* **9**, 90–95 (2007).
62. Waskom, M. et al. mwaskom/seaborn v0.8.0 (Zenodo, 2017); https://doi.org/10.5281/zenodo.824567